Preferential Summer Melt of Deeper Ridge Keels in the Central Arctic Ocean from Multibeam Sonar Data

E. Salganik[1,2], B. A. Lange[2,3], C. Katlein[4], I. Matero[4,5], P. Anhaus[4], M. Muilwijk[2], K. V. Høyland[1], and M. A. Granskog[2]

[1]Norwegian University of Science and Technology, Trondheim, Norway

[2]Norwegian Polar Institute, Fram Centre, Tromsø, Norway

[3]Norwegian Geotechnical Institute, Oslo, Norway

[4]Alfred-Wegener-Institut Helmholtz-Zentrum für Polar- und Meeresforschung, Bremerhaven, Germany

[5]Svalbard Integrated Arctic Earth Observing System Knowledge Centre, Longyearbyen, Svalbard

Corresponding author: Evgenii Salganik (salganikea@gmail.com)

Key Points:

- Sea-ice ridges melt faster than level ice with total snow and ice melt of 1.0 m versus less than 0.6 m respectively in June-July.
- Ridge bottom melt is 3–4 times higher than bottom melt of first-year level ice, while surface melt is almost identical.
- Ridge melt correlates with draft, slope, and width with 57% total contribution, while level ice melt was mostly correlated to its draft.

Plain language summary

The Arctic Ocean is covered by a thin layer of sea ice moved by winds and currents, it can break up, forming piles of broken ice blocks or so-called ridges. Despite ridged ice covering more than a third of the total ice-covered area, they are not as well understood as undeformed level ice, and are not accurately represented in climate models. Sonars are frequently used to investigate submerged objects. Here we measure ice thickness using a sonar attached to an underwater robot. Using these rare measurements, we compare the reduction in ice thickness during summer melt in the Arctic Ocean between deformed and undeformed ice. We show that thicker ridged ice melts two times faster than thinner undeformed ice at both surface and bottom interfaces. We also study how the shape of ridged ice influences how it melts, showing that deeper, steeper, and narrower ridged ice melt the fastest. Additionally, we utilize repetitive temperature measurements to distinguish melting at the boundary of the ice with the atmosphere and the ocean. Our measurements show that deformed ice melts 3–4 times faster than undeformed ice at the bottom ice-ocean boundary, while at the surface they melt at a similar rate.

Abstract

Sea-ice ridges constitute a large fraction of the total Arctic sea-ice volume (up to 40%); nevertheless, they are the least studied part of the Arctic ice pack. Here we investigate sea-ice melt rates using rare underwater multibeam data that cover a period of one month during the advanced melt stage in the Arctic summer. We show that the degree of bottom melt increases with ice draft for first-year and second-year level ice, and a first-year ice ridge keel, with an average of 0.45 m, 0.55 m, and 0.95 m of total snow and ice melt in the observation period, respectively. While bottom melt rates of ridge keels are 3–4 times higher than first-year level ice, surface melt rates are almost identical. Our estimate attributes 57% of the ridge keel melt variability to keel draft (36%), slope (32%), and width (27%).

1 Introduction

According to the definition by the World Meteorological Organization, an ice ridge is a line or wall of broken ice that is forced up by pressure (WMO, 2014). Ridges consist of a sail above and a keel below the water level. The keel initially consists of rubble, randomly packed ice blocks separated by water-filled voids, described by the ridge macroporosity (fraction of water-filled voids in the rubble). The macroporosity of first-year ice ridges is in the range of 20% to 45% (Bowen & Topham, 1996), with an average porosity of 30% (Timco & Burden, 1997). Some ridges become fully consolidated (with near-zero macroporosity) during the melt season (Marchenko, 2022). Ridges that have survived summer melt often have lower macroporosity due to refreezing of meltwater in the ridge keel. Ice ridges are key features in climate studies since they constitute around 30% of the total Arctic sea-ice volume, a fraction which is possibly increasing (Rothrock & Zhang, 2005), partly because they can melt differently in comparison to level ice (Amundrud et al., 2004; Perovich et al., 2003). For example, Melling & Riedel (1996) observed an increase in ridge areal fraction from 15% in autumn to 40–50% in spring based on subsea sonar ice draft measurements in the Beaufort Sea during 1991–1992. Nonetheless, the proportion of ridges varies depending on the region and how they are defined. Hansen et al. (2014) estimated the fraction of thicker ice (predominantly deformed ice) of 37±8%, using an evolving threshold relative to the modal thickness using draft measurements from moored upward- looking sonars in Fram Strait during 1990–2011. In those observations, the ridge fraction increased in 1990–2008 and decreased thereafter, which was confirmed by Sumata et al. (2023) using extended data from the same upward-looking sonars in Fram Strait for 1990 to 2020.

Sea-ice ridges can be formed from new, young, first-year, second-year, or multiyear level ice or from a combination of ice types. Typically, ridges are made from relatively thin ice (Tucker et al., 1984), which breaks as the weakest points during deformation events. Ridges themselves can also be first-year, second-year, or multiyear, depending on how many seasons they have survived. The main characteristics of the ridge morphology are usually correlated despite different mechanisms controlling some of those characteristics. The maximum keel draft is limited by the ice strength and is correlated with adjacent level ice draft (Amundrud et al., 2004). Once the keel has reached its maximum possible draft, it thereafter only grows in width (Hopkins, 1998). In areas with thicker level ice, ridges have higher areal fractions and deeper keels (Samardžija & Høyland, 2023).

Previous research has suggested that ridges impact the melt rates of the ice. For instance, Rigby and Hanson (1976) showed enhanced bottom melt of a ridge keel in comparison to thinner ice, although mechanical erosion could not be ruled out for this rather deep ridge (order of 10–12 m). During the SHEBA expedition, Perovich et al. (2003) used data from ablation stakes, and measured 60% higher bottom melt for ridges than for level ice. Similarly, Skyllingstad et al. (2003) measured enhanced vertical mixing and a five-fold increase in ocean heat flux for 10-m-deep ridges. Amundrud et al. (2006) also estimated that ridge keels melt 5 times faster than level ice based on the observations from ice-profiling sonars mounted on subsea moorings in the Beaufort Sea. Furthermore, Shestov et al. (2018) observed ridge melt in summer during the N-ICE2015 expedition (Granskog et al., 2018) in the pack ice north of Svalbard. Here, the average ocean heat flux under level ice was 63 W m^{-2} (Peterson et al., 2017), while a ridge keel melted by 1.5 m, which translates into an equivalent ocean heat flux of 300 W m^{-2} (Shestov et al., 2018). Based on the thermodynamic model by Amundrud et al. (2006), several parameters, such as keel width and shape, may impact keel melt, with ridge porosity and block thickness being key factors.

The first direct measurements of under-ice topography were linear profiles from narrow-beam upward-looking sonar (Lyon, 1961). However, Wadhams et al. (2006) were the first to use an autonomous underwater vehicle instrumented with a multibeam sonar to study the three-dimensional bottom topography of sea ice in Northeast Greenland. Using multibeam mapping by a submarine, Wadhams & Toberg (2012) found a mean slope of first-year and multi-year ridges of 28° and 25°, respectively. Ekeberg et al. (2015) analyzed the shape of ridge keels using data from upward-looking sonar (single beam) in Fram Strait and suggested that ridges typically have a trapezoidal shape with the bottom width of the keel accounting for an average of 17% of the total keel width.

Although ridges play an important role in the evolution of the Arctic ice pack, ridges are still relatively understudied compared to the level ice that is usually sampled. They have also been identified as potential biological hotspots (Fernández-Méndez et al., 2018; Gradinger et al., 2010) and influencing the light conditions beneath the ice (Katlein et al., 2021). In this study we use rare multibeam ice draft measurements that follow the temporal and spatial evolution of a first-year sea-ice ridge and adjacent level ice during summer melt. The measurements were collected in the central Arctic Ocean during the Multidisciplinary drifting Observatory for the Study of the Arctic

Climate (MOSAiC) expedition in summer 2020 (Nicolaus et al., 2022). Over a period of a month, we measured different ice draft changes and melt rates for first- and second-year level ice and a first-year ice ridge. Additionally, we identified key characteristics of ice bottom topography that affect the melt rates.

2 Materials and Methods

2.1 Ridge drilling

In this study, we focus primarily on the evolution of a ridge called 'Jaridge'. Jaridge was formed between February 4–12, 2020 based on the visual inspection of sea-ice surface elevation models from a helicopter-borne laser scanner (Jutila et al., 2022). The ice blocks forming the ridge were 0.2–0.4 m thick, the average sail height was 0.5 m, and the average draft was 3.8 m. We investigated ridge morphology using a 2-inch diameter ice auger (Kovacs Enterprise, USA). Ice drilling was organized along seven drilling transects perpendicular to the ridge crest orientation (Figure 1a). Each transect contained 3–7 drilling locations with measurements of ice draft, freeboard, depth of ridge voids, and snow thickness at a horizontal spacing of 2.5 or 5 m (Figure 1b). The ridge was measured seven times (June 25 to July 29) during the summer melt season. Jaridge's areal fraction was 12% of the four classified ice types (Figure 1c). Another shallower ridge, 'Porridge' was also located within the survey area but only mapped with the multibeam sonar (Figure 1c). The area at the top right quarter of sonar surveys was heavily covered with false bottoms (Salganik, Katlein, et al., in press) and was therefore excluded from our analysis. Temperature, salinity, and isotope compositions from Jaridge coring are presented in Lange et al. (in review).

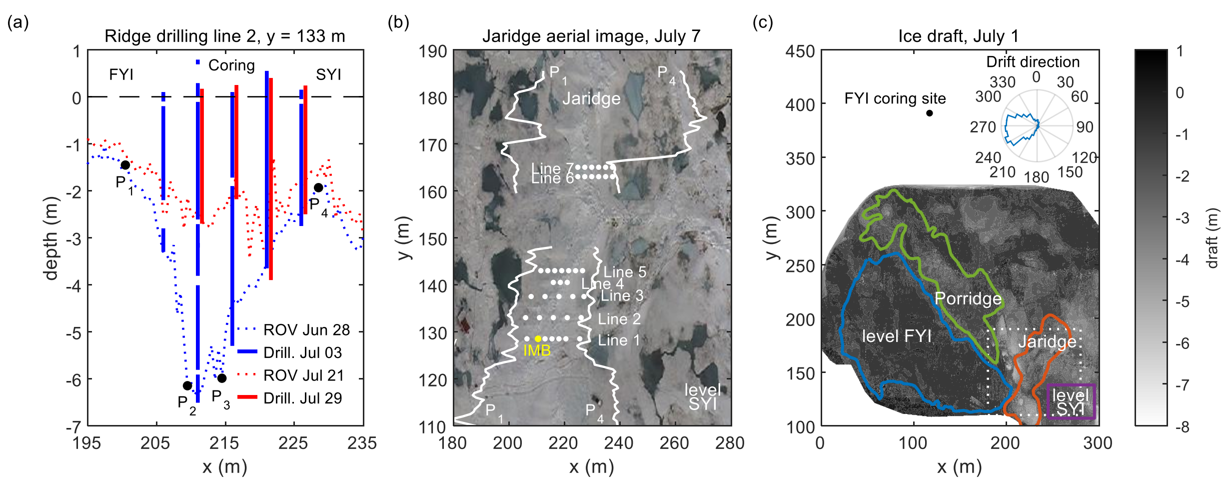

Figure 1. Cross-section of ice draft in late June and late July 2020 along drilling line 2 (a), locations of ridge drillings, temperature buoy (IMB) and keel width interfaces of Jaridge on an aerial image from July 7 (b) and ice bottom topography on July 1, 2020, measured by remotely operated vehicle (ROV) multibeam sonar, showing location of first-year ice (FYI), second-year ice (SYI), Jaridge and Porridge (c) and location of (b) inside white dotted-line box. The polar histogram in (c) shows

frequency of ice drift direction in relation to the displayed ice floe orientation, with prevailing drift in western direction.

To study the temporal evolution of the ridge interfaces, we used temperature measurements from ice mass balance buoy 2020M26 (IMB, Bruncin d.o.o.). The IMB consisted of a 5-m-long chain with a sensor spacing of 2 cm and provides temperature readings every 6 hours with an accuracy of 0.1 °C. The IMB was installed on June 26, 2020 at the ridge drilling Line 1 (Figure 1b). At deployment, the consolidated layer thickness was 1.9 m, keel depth was 4.0 m, and snow depth was 0.6 m. To study the evolution of level ice draft, thickness, and interface evolution, we also used data from the first-year ice (FYI) coring site located 70 m away from the ridge surveys (Figure 1c), further detailed in Salganik, Katlein, et al. (in press). These observations include a combination of sea-ice coring conducted on a weekly basis and IMB temperature measurements. Here we use measurements of FYI temperature, salinity, and density, as well as snow and sea ice thickness and draft from 20–30 sea-ice cores per week.

2.2 Underwater multibeam sonar

We use measurements from a multibeam sonar (DT101, Imagenex, Canada) mounted on a remotely operated vehicle (ROV, M500, Ocean Modules, Sweden, Katlein et al. (2017) to measure the ice draft of an area of approximately 350 m by 200 m, with 0.05 m draft accuracy and horizontal resolution of 0.5 m. Seven surveys at a depth of 20 m were performed during the melt season (June 24 to July 28), close to the floe edge of the Central Observatory of MOSAiC (Nicolaus et al., 2022), covering an area with undeformed ice and several ice ridges including the Jaridge (Figure 1c). The modal draft of open water areas was used as a reference level for zero draft. For the analysis of sea-ice melt evolution, we assume the ratio of ice draft and thickness of 0.9, supported by in situ measurements.

2.3 Ridge morphology analysis

To quantify how ridge characteristics affect the melt rates, we divided our ridge draft multibeam observations into 131 individual cross-sections which were nearly parallel to the direction of ice drift during June–July. The distance between neighboring cross-sections was 0.5 m. We determined the following characteristics for each cross-section: keel bottom width, draft, slope, and distance from the ridge front line. To quantify these parameters with a single value, we simplified each cross-section to a trapezoidal shape following Ekeberg et al. (2015). Four points of these trapezoids (P_1–P_4, Figure 1a) coincide with the largest transition of the smoothed inclination of ridge cross-sections, separating each cross-section into upstream, middle, and downstream edges (locations of P_1 and P_4 are shown in Figure 1b). The upstream edge was facing the ice drift direction, while the downstream edge was on the lee-side of the prevailing ocean current relative to the ice (Figure 1c). The keel bottom width is equal to the horizontal projection of the keel middle part (P_2–P_3), while the keel draft equals to the average draft of the middle part. The keel slope is defined as the angle between the upstream edge and the waterline. A tangent line, “touching” the position of all P_2 points of cross-sections (upstream bottom corners), is the keel edge (Figure 3c). The distance from P_2 of each cross-section to the keel edge was identified as the primary factor for studying ridge melt rates.

3 Results and discussion

3.1 Level ice melt

In this study, we focus on the observed difference in sea-ice draft between the sonar surveys from June 24 to July 21 due to large variability in melt rates. During this period, an area of undeformed FYI (Figure 1c) with an initial draft of 1.4±0.2 m experienced a 0.42±0.26 m decrease in draft, while an area of undeformed SYI with an initial draft of 2.6±0.7 m decreased by 0.50±0.31 m (19% more than FYI). A shallow ridge ('Porridge') with an initial draft of 2.3±0.8 m (similar to SYI) experienced a 0.54±0.61 m decrease in draft.

3.2 Ridge morphology and keel melt

Repeated ridge drilling showed that Jaridge keel melt was inhomogeneous (Figure S1). The average ridge melt along ridge profiles 1–5 was 1.7 m, while ridge flanks melted up to 4.5 m. For the ROV sonar surveys, the average draft change of the ridge area was 0.9±1.0 m with an average initial draft of 3.9±1.1 m (Figure S2). The maximum ridge draft decreased from 8.2 m to 7.0 m, while the largest observed ridge draft reduction was 6.1 m. The average keel slope was 14–15° for both flanks, half of that reported by Wadhams & Toberg (2012), possibly because of larger 5 m minimum draft ridge threshold and triangular ridge shape used in their study. The average fraction of keel bottom width and keel width was 38%, twice as large as the 17% estimated by Ekeberg et al. (2015), which may be related to the larger maximum keel draft (7.2 m in comparison to our 5.3 m). Co-location of ridge draft measurements from drilling and from sonar showed a good agreement of the two draft measurement techniques (R^2 = 0.8) (Figure S3). According to the individual observations of ice draft evolution from sonar, the melt of ridge flanks stronger (1.7 times larger regression slope) depends on ice draft in comparison to the middle part of the ridge keel (Figure 2b). The average melt at the same depth was much higher for flanks than for middle part. For example, for ice draft larger than 4 m, the average draft change for upstream, middle, and downstream edges was 1.3 m, 1.0 m, and 1.4 m, respectively. Figure 2b can be used to predict the ridge melt relative to level ice melt depending on ridge thickness distribution and idealized trapezoidal geometry. On average, ridge flanks and middle parts were melting 1.7 and 2.0 times faster than FYI at the coring site. Higher average melt rate for middle part was related to higher average initial draft for middle part (4.4 m) than for flanks (3.1 m).

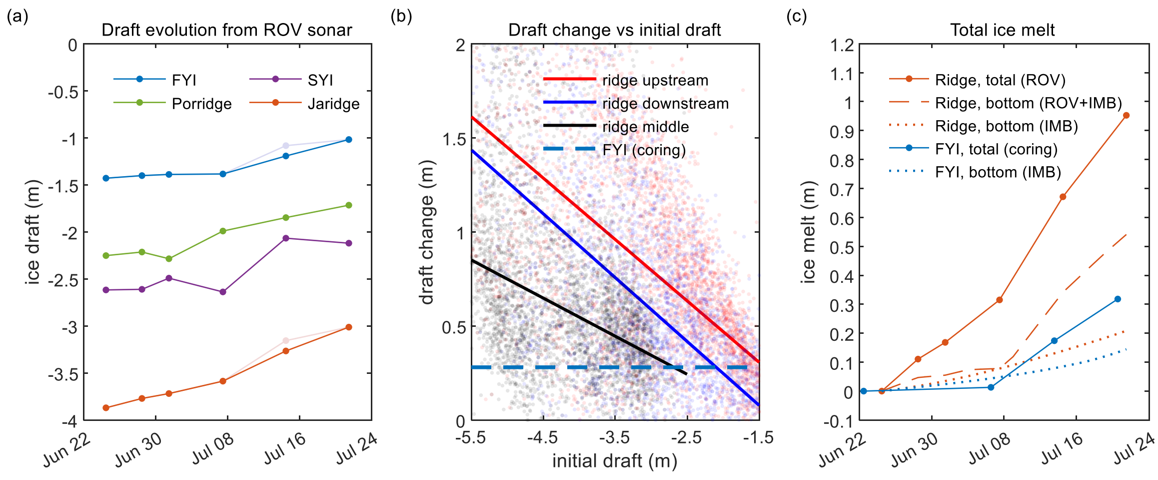

Figure 2. Evolution of the average sea-ice draft measured by a ROV multibeam sonar for first-year ice (FYI), second-year ice (SYI), Porridge and Jaridge during June–July 2020 (a), draft change for single-point sonar measurements of ridge upstream, middle, and downstream edges, corresponding linear regression with solid lines, and average draft change for FYI coring site (b), total ice melt for ridge and FYI estimated from ROV multibeam sonar, ice mass balance buoy (IMB) and ice coring measurements (c). Shaded lines in (a) represent ice draft, not corrected for the melt pond drainage event.

The relationship between sea-ice draft and thickness mainly depends on snow and sea-ice thickness and density. Macfarlane et al. (2021) present an average snow density of 420 kg/m^3 in June and July. Meanwhile, the snow at the FYI coring site melted entirely from an initial depth of 0.08 m. At the FYI coring site, the ratio of ice draft to thickness gradually decreased from 0.92 on June 22 to 0.87 on July 29 (Figure S4). The corresponding estimate of sea-ice bulk density (assuming hydrostatic equilibrium) decreased from 910 kg/m^3 to 876 kg/m^3, which agrees with a sea-ice density decrease from 914 kg/m^3 to 875 kg/m^3 estimated from temperature, density, and salinity measurements performed at the FYI coring site. In these estimates, the gas fraction was calculated from laboratory hydrostatic measurements of sea-ice density, while brine volume was calculated from in situ temperature and salinity measurements. The observed sea-ice density decrease is mainly caused by an increase in gas fraction from 2% to 6%. The ratio of draft to thickness for Jaridge was 0.89±0.06 similar to FYI (Figure S1). The ridge bulk density estimated from laboratory density measurements from July 10 was 892 kg/m^3, which is alike FYI values. These measurements support the 0.9 draft to thickness ratio for analysis of ROV sonar surveys. The average ridge macroporosity (void fraction) measured by drilling in June–July was 4 ± 7% for all

47 drilling sites (Figure S1). This shows that the ridge macroporosity has a minor effect on the estimate of the total volume of melted ice based on its draft measurements.

3.3 Ridge cross-sectional melt

Based on the results of multiple linear regression analysis, keel draft, keel slope, keel bottom-width and distance to the keel edge (Figure 3c) are responsible for 57% of keel melt variability with 37% correlation with keel draft, 32% correlation with keel slope, 27% correlation with keel bottom-width, and 11% correlation with distance from the keel edge. The large correlation of ridge melt with its mean draft may be explained by a combination of both higher ice melt and lower keel width for larger drafts. The negative correlation of keel width with the keel draft is related to the conservation of mass, as most ridge cross-sections were formed from approximately the same volume of ice blocks. Based on observations from Salganik, Lange, et al. (in reveiew), the flanks of ridge keels are usually not consolidated, which may be coupled with higher ocean turbulence at the ridge flanks in comparison to the middle part.

The bottom-width of the keel ranged from 1 m to 35 m with an average of 13 ± 9 m, and the highest melt was observed around their left and right bottom corners (P_2 and P_3) within diameter of 10–12 m. For wide profiles, it was possible to distinguish keel melt around two bottom corners and in the middle part between them. While areas within 10 m around upstream bottom corner (P_2) melted on average by 1.2 m, middle part without 10 m surroundings around both corners (P_2 and P_3) melted by 0.5 m (similar to level ice melt rates despite a much larger ice draft). We also found that all ridge cross-sections that had both narrow bottom-keel width and low keel melt were located within two areas (Figure 3c), and were characterized by large distance from the keel edge. Exclusion of profiles from these two areas increase correlation (R^2) between keel melt and keel bottom-width from 27% to 57% (Figure 3b). We suggest that these areas were protected by the keel front edge from the turbulent fluxes, which appear to occur in the vicinity of ridge keel corners (P_2 and P_3 in Figure 1a).

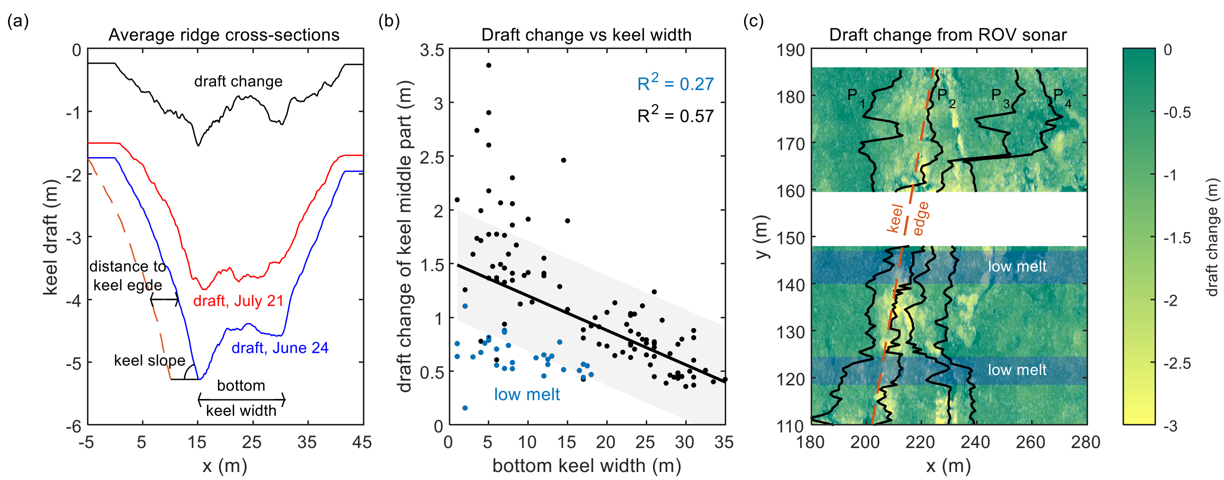

Figure 3. Average ridge cross-section of ice draft in late June and late July 2020 (a), melt of ridge middle part vs bottom keel width for each ridge cross-section (b), contour plot of ridge draft change

from June 24 to July 21 with locations of ridge vortexes (black lines), ridge front line (red line), and cross-sections with low total melt and narrow keel width (blue shaded areas) (c).

3.4 Total, surface and bottom ice melt

In the previous sections we analyzed draft evolution of several sea-ice types. Under the assumption of hydrostatic equilibrium, the sea-ice draft decrease equals the amount of surface and bottom melt multiplied by snow and sea-ice density. Meanwhile, it is important to separate surface and bottom melt to study thermodynamic coupling of sea ice, ocean and atmosphere. From June 22 to July 20, unponded level ice at the FYI coring site experienced 0.21 m surface melt and 0.14 m bottom melt, with nearly identical draft change (0.34 m) and total melt (0.32 m), suggesting a deviation from one-dimensional hydrostatic equilibrium. Meanwhile, sonar measurements of the FYI give a larger draft change (0.41 m), and hence provide a larger estimate of FYI bottom melt (0.25 m). During the same period, the average snow depth above Jaridge decreased from 0.50 m to 0.12 m. Temperature measurements from IMB042 indicate surface ridge sail melt of 0.24 m. Assuming 0.24 m of surface melt and 0.38 m of snowmelt for the whole ridge, using sonar measurements we can estimate the average ridge bottom melt as 0.55 m or 60% of the mean ridge total melt of 0.93 m. This may explain why only 57% of the ridge total melt was related to characteristics of the keel topography. The surface melt of level FYI and the ridge was similar, whereas the ridge bottom melt estimates were 2.2–3.9 times larger than for level FYI. At the IMB location, the measured ridge keel melt, however, was only 0.24 m (from both IMB and ice drilling measurements). These observations do not include ridge internal melt, though, which can give three times larger values of the total ice melt (Salganik, Lange, et al., in revision).

3.5 Effect of meltwater drainage on ice draft

There is a large difference of 0.11 m in estimates of the FYI total melt from coring (0.34 m) and from sonar measurements (0.46 m). We suggest that this difference may be related to the drainage of meltwater, which occured from July 7 to July 14, and was accompanied with the formation of an under-ice meltwater layer with 21% areal coverage and 0.46 m average thickness (Salganik, Katlein, et al., in press). This coincides with the observed meltpond drainage from July 9 to July 13 (Webster et al., 2022). During this period, despite 0.16 m melt there was abnormal 0.08 m increase of FYI freeboard at the coring site. This suggests that the large decrease in draft (0.30 m) for FYI measured by sonar during July 7–14 was not purely due to ice melt, but rather includes approximately 0.10–0.15 m lift (freeboard increase) related to drainage of meltwater. During that period, independent measurements from FYI coring also showed a substantially larger draft decrease (0.24 m in comparison to 0.08 m draft change during July 14–21). Meanwhile, the total FYI melt from coring during these two weeks was 0.16 m and 0.14 m, respectively. Based on FYI coring measurements, ice lift may lead to approximately 0.10–0.15 m overestimation of FYI melt based on sea-ice draft measurements alone. Measurements from a helicopter-borne laser scanner give 0.02 m increase of FYI freeboard during 4–17 July, which agrees with 0.01 m freeboard increase from FYI coring during 6–20 July. This indicates that changes in ice draft and thickness ratio presumably caused by meltwater drainage are reversible. A gradual increase of FYI freeboard from June 22 to July 29 by 0.02 m despite a total FYI melt of 0.52 m, observed at FYI coring site and mainly caused by the decrease of FYI density, may affect aerial and satellite altimetry retrievals in Arctic summer.

Measurements of sea-ice bottom melt allow to estimate the ocean heat flux for different ice types (Text S1). From June 24 to July 21, calculations based on temperature measurements from the FYI IMB result in an average ocean heat flux of 17 Wm^{-2}, increasing from a minimum of 11 Wm^{-2} to a maximum of 36 Wm^{-2}, with a corresponding FYI bottom melt of 0.14 m. A combination of sonar and IMB measurements at the ridge result in an average ocean heat flux of 65 Wm^{-2} with an average of 20 Wm^{-2} during June 24 – July 7 and an average of 107 Wm^{-2} during July 8 – July 21. We suspect that the estimates of FYI bottom melt from sonar measurements may be overestimated due to the complex relationship between FYI draft and thickness during surface melt pond drainage. These processes may affect less the draft measurements of ridges, but could decrease the estimate of the ridge bottom melt from 0.55 m to 0.40–0.45 m. This would result in 2.9–3.8 higher bottom melt rates for the sea-ice ridge than for FYI. Meanwhile, the absence of ridge lift during melt pond drainage is supported by sonar measurements with smaller draft change of FYI and SYI (0.24–0.25 m) right next to the ridge in comparison to the average FYI and SYI draft change of 0.41–0.50 m away from the ridge.

4 Conclusions

We collected a rare dataset using a multibeam sonar mounted on an ROV that captured the three-dimensional change of sea-ice draft over a period of one month during advanced summer melt in the central Arctic Ocean. This revealed that an ice ridge with an average draft of 3.9 m melted faster than adjacent level ice types. The total ridge melt was on average 0.95 m, compared to 0.55 m for level second-year ice and 0.46 m for level first-year ice. These observations can largely be explained by the difference in initial average ice draft, of 1.4 m for first-year level ice, 2.6 m for second-year level ice, and 3.9 m for the ridge keel.

Key factors that affect the melt rates of ridge keels, included the keel draft, slope, width, and distance from the ridge front line. These factors can explain 57% of the total melt variability for this particular ridge, with 36% of the melt variability explained by keel draft, 32% by keel slope, 27% by keel width, and 11% by a distance from the ridge keel edge. We observed a relationship between the melt of ridge flanks with their draft, and amplification of keel melt within 10 m of its bottom edges, while melt rates of the (more level) middle parts of ridge keels were comparable to level ice melt. However, ice draft changes are not all due to ice melt, because the hydrostatic balance of the ice needs to be considered, since, e.g., melt pond drainage and sea-ice density evolution change ice draft. This needs to be taken into account when such measurements are used. Such ice draft changes also affect the ice freeboard and can potentially affect satellite altimetry retrievals in Arctic summer.

Since a large fraction of the Arctic ice pack is made up of deformed (ridged) ice, it is imperative that we better understand the role of ridges in the Arctic sea-ice system. While ridge keels contribute a significant amount of ice melt in summer (Perovich et al., 2021), they also provide a sink for meltwater through refreezing in keel voids (Lange et al., in review; Salganik, Lange, et al., in review). Ridge keels also shape the lateral distribution of under-ice meltwater layers (Salganik et al., in press) and affects turbulent exchanges (Skyllingstad et al., 2003), with implications for ice-ocean exchange (Smith et al., in review). This work showcases areas that warrant future observation-model development for improved representation of ridge related sea-ice processes in models.

Acknowledgments

This work was carried out and data used in this manuscript was produced as part of the international Multidisciplinary drifting Observatory for the Study of the Arctic Climate (MOSAiC) with the tag MOSAiC20192020. We thank all persons involved in the expedition of the Research Vessel Polarstern (Alfred-Wegener-Institut Helmholtz-Zentrum für Polar- und Meeresforschung, 2017) during MOSAiC in 2019–2020 (Project_ID: AWI_PS122_00) as listed in Nixdorf et al. (2021). We would especially like to acknowledge Marcel Nicolaus and Donald Perovich for their effort to coordinate the sea ice physics work during MOSAiC. We are grateful to Marcel Nicolaus for his effort to coordinate ROV work during MOSAiC. We thank Julia Regnery for the assistance with ROV multibeam sonar measurements and ROV co-piloting. We are grateful for the assistance of Niklas Neckel in processing MOSAiC Helicopter-borne RGB orthomosaics.

ES, BAL, KVH, and MAG were supported by the Research Council of Norway through project HAVOC (grant no 280292). BAL and MAG were also supported by Research Council of Norway project CAATEX (grant no 280531) and MAG and MM by the Norwegian Polar Institute. MAG and MM received funding from the European Union's Horizon 2020 research and innovation programme (grant agreement No 101003826) via project CRiceS (Climate Relevant interactions and feedbacks: the key role of sea ice and Snow in the polar and global climate system). ROV operations, IM and CK were jointly supported by UKRI Natural Environment Research Council (NERC) and the German Federal Ministry of Education and Research (BMBF) through the Diatom ARCTIC project (BMBF Grant 03F0810A). ROV operations were further supported by the Helmholtz Infrastructure Initiative Frontiers in Arctic marine Monitoring (FRAM). PA was supported through the Alfred-Wegner-Institutes internal project AWI_ROV and BMBF through the Diatom ARCTIC project (BMBF Grant 03F0810A) and the IceScan project (BMBF Grant 03F0916A).

Open Research

All scientific data used in this study is publicly available:

Granskog, M. A.; Lange, B. A., Salganik, E., De La Torre, P. R., Riemann-Campe, K. (2021). Temperature and heating induced temperature difference measurements from the modular buoy 2020M26, deployed during MOSAiC 2019/20. *PANGAEA*, https://doi.org/10.1594/PANGAEA.938354

Jutila, A., Hendricks, S., Birnbaum, G., von Albedyll, L., Ricker, R., Helm, V., Hutter, N., Haas, C. (2022). Geolocated sea-ice or snow surface elevation point cloud segments from helicopter-borne laser scanner during the MOSAiC expedition, version 1. *PANGAEA*, https://doi.pangaea.de/10.1594/PANGAEA.950509

Katlein, C., Anhaus P., Arndt S., Krampe, D., Lange, B. A., Matero, I., Regnery, J., Rohde, J., Schiller, M., Nicolaus, M. (2022). Sea-ice draft during the MOSAiC expedition 2019/20. *PANGAEA*, https://doi.org/10.1594/PANGAEA.945846

Lange, B. A., Salganik, E., Macfarlane, A. R., Schneebeli, M., Høyland, K. V., Gardner, J., Müller, O., Granskog, M. A. (2022). Ridge ice oxygen and hydrogen isotope data MOSAiC Leg 4 (PS122/4). *PANGAEA*, https://doi.org/10.1594/PANGAEA.943746

Macfarlane, A. R., Schneebeli, M., Dadic, R., Wagner, D. N., Arndt, S., Clemens-Sewall, D., Hämmerle, S., Hannula, H.-R., Jaggi, M., Kolabutin, N., Krampe, D., Lehning, M., Matero, I., Nicolaus, M., Oggier, M., Pirazzini, R., Polashenski, C., Raphael, I., Regnery, J., Shimanchuck, E., Smith, M. M., Tavri, A. (2021). Snowpit raw data collected during the MOSAiC expedition. PANGAEA, https://doi.org/10.1594/PANGAEA.935934

Neckel, N., Fuchs, N., Birnbaum, G., Hutter, N., Jutila, A., Buth, L., von Albedyll, L., Ricker, R., Haas, C. 2022. Helicopter-borne RGB orthomosaics and photogrammetric Digital Elevation Models from the MOSAiC Expedition. *PANGAEA*, https://doi.pangaea.de/10.1594/PANGAEA.949433

Oggier, M., Salganik, E., Whitmore, L., Fong, A. A., Hoppe, C. J. M., Rember, R., Høyland, K. V., Divine, D. V., Fons, S. W., Abrahamsson, K., Aguilar-Islas, A. M., Angelopoulos, M., Balmonte, J. P., Bozzato, D., Bowman, J. S., Chamberlain, E., Creamean, J., D'Angelo, A., Gardner, J., Haapala, J., Immerz, A., Kolabutin, N., Lange, B. A., Lei, R., Marsay, C. M., Maus, S., Olsen, L. M., Müller, O., Ren, J., Rinke, A., Sheikin, I., Shimanchuk, E., Spahic, S., Torres-Valdés, S., Torstensson, A., Ulfsbo, A., Wang, L., Granskog, M. A. (2023). First-year sea-ice salinity, temperature, density, oxygen and hydrogen isotope composition from the main coring site (MCS-FYI) during MOSAiC legs 1 to 4 in 2019/2020. PANGAEA, https://doi.pangaea.de/10.1594/PANGAEA.956732

Salganik, E., Lange, B. A., Sheikin, I., Høyland, K. V., Granskog, M. A. (2023). Drill-hole ridge ice and snow thickness and draft measurements of "Jaridge" during MOSAiC 2019/20. *PANGAEA*, https://doi.org/10.1594/PANGAEA.953880

Salganik, E., Lange, B. A., Høyland, K. V., Gardner, J., Müller, O., Tavri, A., Mahmud, M. Granskog, M.A. (2023): Ridge ice density data MOSAiC Leg 4 (PS122/4). PANGAEA, https://doi.org/10.1594/PANGAEA.953865

Schmithüsen, H. 2021. Continuous meteorological surface measurement during POLARSTERN cruise PS122/4. Alfred Wegener Institute, Helmholtz Centre for Polar and Marine Research, Bremerhaven, PANGAEA, https://doi.org/10.1594/PANGAEA.935224

Schulz, K., Mohrholz, V., Fer, I., Janout, M. A., Hoppmann, M., Schaffer, J., Koenig, Z., Rabe, B., Heuzé, C., Regnery, J., Allerholt, J., Fang, Y.-C., He, H., Kanzow, T., Karam, S., Kuznetsov,

I. Kong, B., Liu, H., Muilwijk, M., Schuffenhauer, I., Sukhikh, N., Sundfjord, A., Tippenhauer, S. (2022): Microstructure profiler raw data (MSS091) during legs 4 and 5 of the MOSAiC expedition in 2020. *PANGAEA*, https://doi.org/10.1594/PANGAEA.939795

References

Amundrud, T. L., Melling, H., & Ingram, G. (2004). Geometrical constraints on the evolution of ridged sea ice. *Journal of Geophysical Research: Oceans*, *109*(6), 1–12. https://doi.org/10.1029/2003JC002251

Amundrud, T. L., Melling, H., Ingram, R. G., & Allen, S. E. (2006). The effect of structural porosity on the ablation of sea ice ridges. *Journal of Geophysical Research*, *111*(C6), C06004. https://doi.org/10.1029/2005JC002895

Bowen, R. G., & Topham, D. R. (1996). A study of the morphology of a discontinuous section of a first year arctic pressure ridge. *Cold Regions Science and Technology*, *24*(1), 83–100. https://doi.org/10.1016/0165-232X(95)00002-S

Ekeberg, O., Høyland, K., & Hansen, E. (2015). Ice ridge keel geometry and shape derived from one year of upward looking sonar data in the Fram Strait. *Cold Regions Science and Technology*, *109*, 78–86. https://doi.org/10.1016/j.coldregions.2014.10.003

Fernández-Méndez, M., Olsen, L. M., Kauko, H. M., Meyer, A., Rösel, A., Merkouriadi, I., et al. (2018). Algal Hot Spots in a Changing Arctic Ocean: Sea-Ice Ridges and the Snow-Ice Interface. *Frontiers in Marine Science*, *5*. https://doi.org/10.3389/fmars.2018.00075

Gradinger, R., Bluhm, B., & Iken, K. (2010). Arctic sea-ice ridges—Safe heavens for sea-ice fauna during periods of extreme ice melt? *Deep Sea Research Part II: Topical Studies in Oceanography*, *57*(1–2), 86–95. https://doi.org/10.1016/j.dsr2.2009.08.008

Granskog, M. A., Fer, I., Rinke, A., & Steen, H. (2018). Atmosphere-Ice-Ocean-Ecosystem Processes in a Thinner Arctic Sea Ice Regime: The Norwegian Young Sea ICE (N-ICE2015) Expedition. *Journal of Geophysical Research: Oceans*, *123*(3), 1586–1594. https://doi.org/10.1002/2017JC013328

Hansen, E., Ekeberg, O. -C., Gerland, S., Pavlova, O., Spreen, G., & Tschudi, M. (2014). Variability in categories of Arctic sea ice in Fram Strait. *Journal of Geophysical Research: Oceans*, *119*(10), 7175–7189. https://doi.org/10.1002/2014JC010048

Hopkins, M. A. (1998). Four stages of pressure ridging. *Journal of Geophysical Research: Oceans*, *103*(C10), 21883–21891. https://doi.org/10.1029/98JC01257

Katlein, C., Schiller, M., Belter, H. J., Coppolaro, V., Wenslandt, D., & Nicolaus, M. (2017). A New Remotely Operated Sensor Platform for Interdisciplinary Observations under Sea Ice.

Frontiers in Marine Science, *4*, 1–12. https://doi.org/10.3389/fmars.2017.00281

Katlein, C., Langelier, J., Ouellet, A., Lévesque-Desrosiers, F., Hisette, Q., Lange, B. A., et al. (2021). The Three-Dimensional Light Field Within Sea Ice Ridges. *Geophysical Research Letters*, *48*(11). https://doi.org/10.1029/2021GL093207

Lange, B. A., Salganik, E., Macfarlane, A., Schneebeli, M., Høyland, K. V., Gardner, J., et al. (n.d.). Snowmelt contributes to Arctic first-year ice ridge mass balance and rapid consolidation during summer melt. *Elementa: Science of the Anthropocene*, (in review).

Lyon, W. (1961). Ocean and sea-ice research in the Arctic Ocean via submarine. *Transactions of the New York Academy of Sciences*, *23*(8 Series II), 662–674. https://doi.org/10.1111/j.2164-0947.1961.tb01400.x

Marchenko, A. (2022). *Thermo-Hydrodynamics of Sea Ice Rubble*. *IUTAM Bookseries* (Vol. 39). Springer International Publishing. https://doi.org/10.1007/978-3-030-80439-8_10

Melling, H., & Riedel, D. A. (1996). Development of seasonal pack ice in the Beaufort Sea during the winter of 1991-1992: A view from below. *Journal of Geophysical Research: Oceans*, *101*(C5), 11975–11991. https://doi.org/10.1029/96JC00284

Nicolaus, M., Perovich, D. K., Spreen, G., Granskog, M. A., von Albedyll, L., Angelopoulos, M., et al. (2022). Overview of the MOSAiC expedition. *Elementa: Science of the Anthropocene*, *10*(1). https://doi.org/10.1525/elementa.2021.000046

Perovich, D., Smith, M., Light, B., & Webster, M. (2021). Meltwater sources and sinks for multiyear Arctic sea ice in summer. *Cryosphere*, *15*(9), 4517–4525. https://doi.org/10.5194/tc-15-4517-2021

Perovich, D. K., Grenfell, T. C., Richter-Menge, J. A., Light, B., Tucker, W. B., & Eicken, H. (2003). Thin and thinner: Sea ice mass balance measurements during SHEBA. *Journal of Geophysical Research: Oceans*, *108*(3), 1–21. https://doi.org/10.1029/2001jc001079

Peterson, A. K., Fer, I., McPhee, M. G., & Randelhoff, A. (2017). Turbulent heat and momentum fluxes in the upper ocean under Arctic sea ice. *Journal of Geophysical Research: Oceans*, *122*(2), 1439–1456. https://doi.org/10.1002/2016JC012283

Rigby, F. A., & Hanson, A. (1976). Evolution of a large Arctic pressure ridge. *AIDJEX Bull.*, *34*, 43–71. Retrieved from http://psc.apl.washington.edu/nonwp_projects/aidjex/files/AIDJEX-34.pdf

Rothrock, D. A., & Zhang, J. (2005). Arctic Ocean sea ice volume: What explains its recent depletion? *Journal of Geophysical Research: Oceans*. https://doi.org/10.1029/2004JC002282

Salganik, E., Lange, B. A., Itkin, P., Divine, D., Katlein, C., Nicolaus, M., et al. (n.d.). Different mechanisms of Arctic first-year sea-ice ridge consolidation observed during the MOSAiC expedition. *Elementa: Science of the Anthropocene, in review*.

Salganik, E., Katlein, C., Lange, B. A., Matero, I., Ruibo, L., Fong, A. A., et al. (2023). Temporal evolution of under-ice meltwaterlayersand false bottomsand their impact on summer Arctic sea ice mass balance. *Elementa: Science of the Anthropocene, in press*. https://doi.org/10.31223/X5H37R

Samardžija, I., & Høyland, K. V. (2023). Analysis of the relationship between level ice draft, ridge frequency and ridge keel draft for use in the probabilistic assessment of ice ridge loads on offshore structures. *Ocean Engineering*, *270*, 113593. https://doi.org/10.1016/j.oceaneng.2022.113593

Shestov, A., Høyland, K., & Ervik, Å. (2018). Decay phase thermodynamics of ice ridges in the Arctic Ocean. *Cold Regions Science and Technology*, *152*(December 2017), 23–34. https://doi.org/10.1016/j.coldregions.2018.04.005

Skyllingstad, E. D., Paulson, C. A., & Pegau, W. S. (2003). Effects of keels on ice bottom turbulence exchange. *Journal of Geophysical Research*, *108*(C12), 3372. https://doi.org/10.1029/2002JC001488

Sumata, H., de Steur, L., Divine, D. V., Granskog, M. A., & Gerland, S. (2023). Regime shift in Arctic Ocean sea ice thickness. *Nature*, *615*(March), 443–449. https://doi.org/10.1038/s41586-022-05686-x

Timco, G. W., & Burden, R. P. (1997). An analysis of the shapes of sea ice ridges. *Cold Regions Science and Technology*, *25*(1), 65–77. https://doi.org/10.1016/S0165-232X(96)00017-1

Tucker, W. B., Sodhi, D. S., & Govoni, J. W. (1984). Structure of first-year pressure ridge sails in the Prudhoe region. In *The Alaskan Beaufort Sea* (pp. 115–135). Elsevier. https://doi.org/10.1016/B978-0-12-079030-2.50012-5

Wadhams, P., Wilkinson, J. P., & McPhail, S. D. (2006). A new view of the underside of Arctic sea ice. *Geophysical Research Letters*, *33*(4), L04501. https://doi.org/10.1029/2005GL025131

Wadhams, Peter, & Toberg, N. (2012). Changing characteristics of arctic pressure ridges. *Polar Science*, *6*(1), 71–77. https://doi.org/10.1016/j.polar.2012.03.002

Webster, M. A., Holland, M., Wright, N. C., Hendricks, S., Hutter, N., Itkin, P., et al. (2022). Spatiotemporal evolution of melt ponds on Arctic sea ice. *Elementa: Science of the Anthropocene*, *10*(1). https://doi.org/10.1525/elementa.2021.000072

WMO. (2014). *World Meteorological Organization (WMO) Sea Ice Nomenclature: WMO-No. 259 922. Supplement to Vol. I, II and II, 5th session of JCOMM Expert Team on Sea ice. Tech.*

rep. https://doi.org/10.25607/OBP-1530